UDC 621.039.51
IRSTI 58.33.29

https://doi.org/10.55452/1998-6688-2026-23-2-401-417

[1]Aryngazin A.,
MSc, ORCID ID: 0009-0007-7861-4917,
e-mail: ansar.aryngazin@nu.edu.kz
[1]Kurbanova B.,
MSc, ORCID ID: 0000-0003-0928-521X,
e-mail: bayan.kurbanova@nu.edu.kz
[2]Sizyuk Y.,
PhD, e-mail: yuriy.sizyuk@nu.edu.kz
[3]Temirbayeva A.
M.Sc., ORCID ID: 0000-0002-9526-3617,
e-mail: assem.zkgmu@gmail.com
[1]Alsar Zh.,
PhD, ORCID ID: 0000-0001-7287-7555,
e-mail: zhanna.alsar@nu.edu.kz
[1]*Insepov Z.,
D.Sc. PhD, Adj. Professor, ORCID ID: 0000-0002-8079-6293,
*e-mail: zinsepov@nu.edu.kz

[1]Nazarbayev University Research Administration, Astana, Kazakhstan
[2]Depart. Mech. Nucl. Engin, Virginia Commonwealth University, VA USA
[3]Eurasian National University named after Gumilev, Astana, Kazakhstan
[4]School of Nuclear Engineering, Purdue University IN, USA

NEUTRONICS AND THERMAL-HYDRAULICS OF PRESSURIZED WATER REACTOR WITH THORIUM-BASED FUEL

Abstract

In the present study, the coupled behavior of thermal-hydraulic processes and solid mechanics phenomena was investigated using the finite element method implemented within the COMSOL Multiphysics environment. Neutronic analyses were performed using the OpenMC code under the steady-state neutron transport approximation. To optimize the core configuration of a thorium-fueled pressurized water reactor (PWR), high-pressure light water was selected as the coolant and moderator. The reactor core was composed of 49 fuel rods containing thorium-based fuel compounds arranged in a regular lattice configuration. Monte Carlo neutron transport simulations conducted with OpenMC enabled the evaluation of the effective neutron multiplication factor (k_eff) and the spatial power distribution within the reactor core. Thermal-hydraulic calculations yielded detailed temperature and coolant velocity distributions, while solid mechanics analyses provided the corresponding spatial distributions of stresses and deformations arising under operational conditions. The obtained results demonstrate the applicability and effectiveness of a coupled multiphysics approach integrating steady-state neutronics with thermal-hydraulic and structural analyses for the assessment and optimization of thorium-fueled pressurized water reactor systems.

Keywords: nuclear reactor physics, thorium fuel, neutronics, thermal-hydraulics, solid mechanics, COMSOL, OpenMC.

Received February 25, 2026; revised May 28, 2026; accepted June 9, 2026.

1. Introduction

The growing demand for sustainable and proliferation-resistant nuclear energy systems has stimulated renewed interest in alternative fuel cycles capable of improving resource utilization and reducing long-lived radioactive waste. Among such alternatives, thorium-based fuels have attracted considerable attention due to their favorable neutronic characteristics, high natural abundance, and potential for reduced production of minor actinides compared with conventional uranium fuel cycles [1]. The thorium fuel cycle has been studied for several decades, beginning with early experimental demonstrations such as the Molten Salt Reactor Experiment conducted at Oak Ridge National Laboratory in the 1960s [2]. Since then, numerous investigations have explored the feasibility of incorporating thorium into both existing and advanced reactor systems.

In light-water reactors, and particularly in pressurized water reactors (PWRs), partial or full replacement of uranium fuel with thorium-based compositions has been proposed as a promising pathway toward improved fuel utilization and waste reduction. Thorium dioxide exhibits several advantageous thermophysical properties, including higher thermal conductivity and lower thermal expansion compared with uranium dioxide [1]. These characteristics can contribute to reduced temperature gradients, improved thermal margins, and enhanced structural stability of fuel elements during operation. At the same time, incorporation of fissile isotopes such as U-233 or low-enriched uranium enables thorium to sustain nuclear fission through neutron capture and subsequent transmutation processes.

Previous studies have investigated neutronic performance, burnup characteristics, and safety parameters of thorium-based fuels in thermal and fast reactor systems. Monte Carlo transport simulations using codes such as MCNP [3, 4] and OpenMC [5], supported by evaluated nuclear data libraries including ENDF [6] and JEFF [7], have demonstrated the feasibility of thorium utilization in PWR assemblies with acceptable reactivity coefficients and fuel cycle performance [8–17]. In parallel, thermal-hydraulic and thermo-mechanical analyses have shown that the superior thermal conductivity of ThO_2-based fuels can reduce peak fuel temperatures and mitigate fuel-cladding mechanical interaction [18–25]. However, most existing investigations treat neutronics, thermal-hydraulics, and structural behavior either independently or within simplified coupling frameworks, which may limit the accuracy of safety and performance assessments.

Accurate prediction of reactor behavior requires consistent coupling between neutronic power generation and the resulting thermal-hydraulic and mechanical responses of the fuel system. While time-dependent neutronic simulations provide detailed transient behavior, they are computationally expensive when combined with high-fidelity multiphysics models [26–28]. An alternative approach involves coupling steady-state neutronics with transient thermal-hydraulic and structural calculations [29, 30]. This approach exploits the difference in characteristic timescales between neutron transport and thermal-hydraulic processes: neutron populations typically reach equilibrium much faster than temperature and flow fields evolve. As a result, steady-state neutronic solutions can be used to provide spatial power distributions that drive time-dependent thermal and mechanical simulations with significantly reduced computational cost.

Such multiphysics coupling has been applied in recent years to both conventional light-water reactors and advanced reactor concepts [26, 29, 31]. Studies indicate that steady-state neutronics combined with transient thermal-hydraulics can provide reliable predictions of temperature evolution, stress development, and flow stability while maintaining acceptable computational efficiency. Nevertheless, further investigation is required to assess the applicability of this approach to thorium-based fuel assemblies in PWR configurations and to evaluate the resulting thermo-mechanical behavior under transient heating conditions.

By combining steady-state neutronics with time-dependent thermal-hydraulic and structural modeling, this study aims to provide a consistent multiphysics assessment of thorium-based fuel

performance in a PWR assembly and to evaluate the suitability of this coupling strategy for future high-fidelity reactor safety analyses.

In this paper a Design-Basis Core of a conventional PWR with Thorium/Uranium Oxide fuel, Zircaloy-4 cladding and light water coolant was considered. The neutronics study was performed using OpenMC v.0.15.3 with ENDF.B.VIII-0 nuclear cross-section library data. The thermal-hydraulics, solid mechanics and fuel safety study were performed in COMSOL v.6.3. The paper is organized as follows: Section II describes main methods and materials used for the study. In Section III the results are obtained and discussed. In Section IV conclusions and future research goals are presented.

2. Methods and models

2.1. OpenMC

OpenMC is an open-source community-developed Monte-Carlo neutron and photon transport simulation software package. It uses constructive solid geometry or CAD representation to perform various neutronics calculations with capabilities of computation parallelism via MPI, OpenMP or hybrid programming model [5].

The model in consideration of neutronics calculations is an assembly of 7x7 pins arranged in rectangular lattice with $(Th/^{233}U)O_2$ fuel domain, enveloped by Zircaloy-4 alloy as a cladding domain. These pillars are surrounded by light water coolant domain. Featured important specifications of a reactor core are listed in Table 1. The top view slice at half-height of the assembly can be seen in Figure 1.

Table 1 – Parameters of a PWR Design Core

Parameter	Value
Core lattice geometry	Rectangular
Number of pins	49 (7x7)
Fuel material	$(Th_{0.985}, ^{233}U_{0.015}$ at%$)O_2$
Fuel density	10.0 g/cm^3
Fuel temperature	900 K
Fuel thickness	1 cm
Fuel element height	100 cm
Cladding material	Zircaloy-4 ($Zr_{0.985}Sn_{0.014}5Fe_{0.0021}Cr_{0.0009}$ at%)
Cladding density	6.55 g/cm^3
Cladding thickness	0.2 cm
Coolant material	H_2O
Coolant density	1.0 g/cm^3
Boundaries	X: -0.75 – +21.75 cm Y: -0.75 – +21.75 cm Z: -50 – +50 cm
Active core volume	50 625 cm^3
Mesh dimensions	500x500x500

The calculations parameters have been chosen to optimize between the complexity and accuracy and time of calculations that depends on computing power of processing units. According to execution settings for the specific OpenMC mode called “k-eigenvalue”, a single run simulates a selected by the user number of particles, that combine into fission generations that store resulting fission neutrons,

the spatial coordinates of the fission site, the sampled outgoing energy and direction of the fission neutron, and the weight of the neutron of the current generation. Then, the next successive generation uses random sampling of stored generation to ensure that the neutron population won't grow in a rapid manner. Successive generations combine into batches for statistical significance. Some batches are needed to be discarded in order for the source – not known a priori – to evolve closer to true distribution at each iteration. After that the tallies that contain execution information are starting to accumulate. In the simulations presented here, 96000 particles with 25 generations per batch, 240 batches and 100 inactive batches were used.

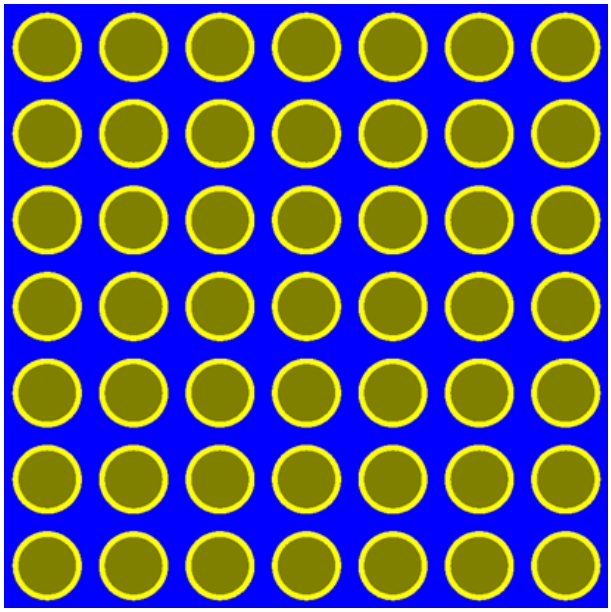

Figure 1 – 2D slice of a PWR Design Core at half-height of the design core.
Designations: blue – coolant, yellow – cladding, olive – fuel

For the accurate calculations of neutron flux and heat distribution throughout the assembly without heavy overstress of processing power the assembly space was divided into 3D mesh with moderate resolution of 60 blocks per dimension. This value ensures enough accuracy for calculations while providing easiness on post-processing of obtained raw results.

Additionally in the execution settings, a source of neutrons constrained inside the fuel only domain with uniform spatial distribution, isotropic angular distribution, Watt energy distribution and strength of source at 98% was included. To get the analogous perspective of neutron energy spectrum from similar reactor cores, the closest to PWR cross-section data library available, called SHEM-361, was used.

2.2. Thermal-hydraulics and solid mechanics with COMSOL

The radial power distribution from the neutronic analysis is used to perform thermal-hydraulic and solid-mechanics simulations. The objective is to capture and analyze these conditions through numerical simulations.

Based on the power distribution, the hottest fuel rod can be identified, representing the most limiting and safety-critical operating conditions within the reactor core. The solution procedure begins with discretizing the geometry into smaller elements, a process referred to as meshing. Subsequently, the governing partial differential equations (PDEs) are applied to the generated mesh. The heat transfer equation is:

$$\rho C_p \left(\frac{\partial T}{\partial t} + u_{trans} \cdot \nabla T\right) + \nabla \cdot q = Q + Q_{ted} \quad (1)$$

where equation parameters are listed in Table 2.

Table 2 – Heat transfer equation parameters

Parameter	Unit	Definition
ρ	kg/m^3	Density
C_p	$J/(kg \cdot K)$	specific heat at constant pressure
T	K	Temperature
u_{trans}	m/s	velocity vector of translational motion
$q = -k\nabla T$	W/m^2	conduction heat flux
k	$W/(m \cdot K)$	Thermal conductivity
Q	W/m^3	additional heat sources
$Q_{ted} = \alpha T : \frac{dS}{dt}$	W/m^3	thermoelastic damping term
α	$1/K$	thermal expansion coefficient
S	Pa	Piola–Kirchhoff stress tensor
$d/dt = \partial/\partial t + u \cdot \nabla$	$1/s$	Material derivative

and : stands for double-dot tensor product (double contraction).

A free triangular fine mesh was employed in the simulations and is illustrated in Figure 2.

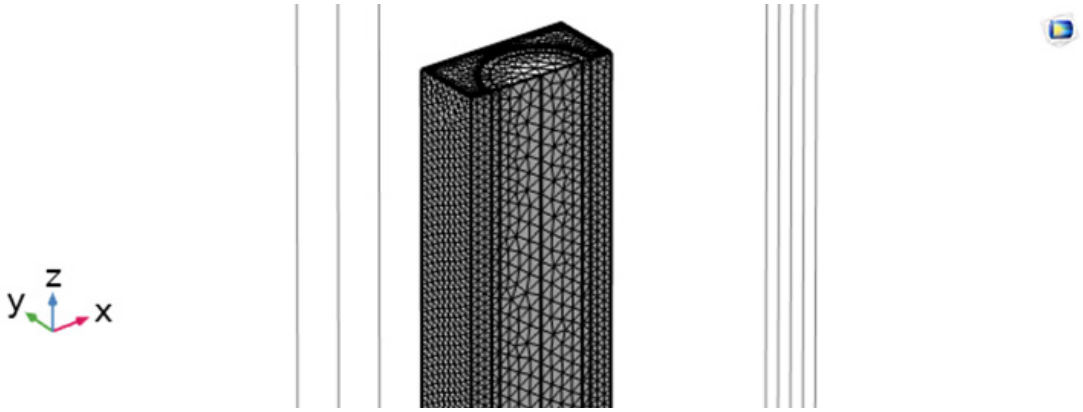

Figure 2 – Mesh of the single pint, from inward:
1 – fuel rod, 2 – cladding and 3 – coolant

With the thermal power applied as a heat source over the cross-sectional surface of the core, the equation (1) is solved using the finite element methods to determine the spatial temperature distribution within the fuel, cladding, and coolant regions. Heat generation was applied only in the fuel domain, while heat transfer through the fuel–cladding and cladding–coolant interfaces was solved by the coupled heat-transfer and fluid-flow physics. All boundaries are assumed to be thermally insulated, except for the top, bottom, and cross-sectional surfaces and are explicitly formulated as follows:

$$-n \cdot q = 0, \quad (2)$$

where n is a vector normal to the surface.

The adiabatic boundary condition was applied only to the external lateral boundaries of the computational domain to avoid artificial heat losses from the selected fuel-rod/coolant subdomain. This assumption represents a simplified local-domain approximation and does not suppress heat transfer between the fuel, cladding, and coolant. Convective heat removal was modeled explicitly through the coupled heat-transfer and turbulent-flow interfaces in the coolant region, with inlet and outlet boundaries imposed at the bottom and top surfaces, respectively

Thermal properties of fuel [32] and clad materials [33] as temperature-dependent expressions are listed in Table 3.

Table 3 – Thermodynamical properties of fuel and cladding as temperature-dependent polynomials

	$(Th, ^{233}U)O_2$	Zircaloy-4
C_p	$239.9 + 8.512 \times 10^{-5} \cdot T$ $-5.754 \times 10^{-8} \cdot T^2$ $+1.528 \times 10^{-11} T^3$ [J/(mol · K)]	$7.1 \cdot 10^{-2}$ $+1.7 \cdot 10^{-5} \cdot T$ $-0.89 \cdot 10^{-3} \cdot T^2$ [cal/g · K]
k	14.242 $-0.022 \cdot T$ $+1.764 \times 10^{-5} \cdot T^2$ $-6.380 \times 10^{-9} \cdot T^3$ $+8.038 \times 10^{-13} \cdot T^4$[W/(m · K)]	0.11804 $+0.00012 \cdot T$ $-4.33441 \cdot 10^{-8} \cdot T^2$ $+5.90277 \times 10^{-11} \cdot T^3$ [W/(cm · °C)]
ρ	9326 $- 0.0004 \cdot T$ $+2.54 \times 10^{-7} \cdot T^2$ $-7.897 \times 10^{-11} \cdot T^3$ [kg/m³]	10950 $- 0.35 \cdot T$ $- 1.2 \cdot 10^{-4} \cdot T^2$ [kg/m³]

The Navier–Stokes PDE governing momentum and mass conservation are solved to obtain the coolant pressure along the axial (z) direction as well as the corresponding velocity field – see Equation 3:

$$\rho \frac{\partial^2 u}{\partial t^2} = \nabla \cdot \sigma + F_v, \tag{3}$$

where equation parameters are listed in Table 4.

Table 4 – Navier-Stokes equation parameters

Parameter	Unit	Definition
ρ	kg/m³	Mass density
u	J/(kg · K)	Displacement field
σ	Pa	Cauchy stress tensor
F_v	N	Body force

When the turbulent flow (k–ω) model is coupled with the heat-transfer physics, two key quantities are determined: (i) the convective heat-transfer coefficient h, which depends on the coolant velocity, channel geometry, and temperature-dependent coolant properties, and (ii) the axial pressure

drop resulting from the Navier–Stokes solution. The coolant flow was prescribed through the axial direction of the fuel-rod channel. The bottom surface of the coolant domain was defined as the inlet, where the inlet velocity and coolant temperature were specified. The top surface was defined as the outlet, where pressure was fixed to the reference outlet pressure. No-slip wall conditions were applied at the solid–fluid interfaces.

Coupled equation determines influence of thermal expansion on material's strain:

$$\varepsilon_{th} = \alpha(T)(T - T_{ref}) \quad (4)$$

Within the solid mechanics interface, the governing elasticity equations are solved to evaluate thermally induced deformation, displacement, and strain in the fuel and cladding, fully coupled with the heat-transfer physics. The fuel and cladding domains were coupled to the temperature field obtained from the heat-transfer calculation. Thermally induced expansion was included through the temperature-dependent thermal expansion coefficient. The top and bottom boundaries of the solid domain were mechanically constrained to represent axial support of the fuel rod, while the remaining surfaces were allowed to deform freely unless otherwise specified. This setup allows evaluation of thermally induced displacement, volumetric strain, and von Mises stress under constrained axial conditions

For mechanical properties, the following thermal expansion expressions for fuel [34] and clad [32], presented in Table 5, were used:

Table 5 – Mechanical properties of fuel and cladding as temperature-dependent polynomials

	$(Th, ^{233}U)O_2$	Zircaloy-4
α	$5.416 \cdot 10^{-6} + 3.47 \cdot 10^{-9} \cdot T + 3.0107 \cdot 10^{-15} \cdot T^2 - 1.2212 \cdot 10^{-15} \cdot T^3 + 4.181 \cdot 10^{-19} \cdot T^4$ [1/K]	$(5.22 + 1.82 \cdot 10^{-3} \cdot T) \cdot 10^{-6}$[1/K]
E	$259.87 \cdot 10^9 \cdot (1 - P^2)$ [Pa]	$9.21 \cdot 10^{10} - 4.05 \cdot 10^7 \cdot T$ [Pa]

where P is the porosity of material.

3. Results and Discussion

3.1. Effective neutron multiplication coefficient, heat power distribution and peak power density

The maximum normalized heating density value has been obtained:

$$\omega = 4109.2892 \text{ W/cm}^3.$$

In this work, the hottest fuel rod was selected based on the OpenMC volumetric power distribution, and the maximum normalized heating volumetric density value was used in COMSOL to represent the most limiting thermal-hydraulic and thermo-mechanical condition. The maximum value was selected because it corresponds to the hottest fuel rod and it represents the most safety-critical location in the core, where the highest temperature, thermal stress, strain, and displacement are expected.

Effective multiplication coefficient $k_{eff} = 1.01777 \pm 0.00005$. Normalized neutron spectrum of the model in comparison with SHEM-361 is presented in Figure 3. The values of the flux are significantly higher for the model than for the reference group. This is explained by a multitude of factors, despite SHEM-361 being suitable for comparison of various LWR reactors: geometry or tally

constraints – as tallies for the calculations were constrained only in the fuel domain, and energy-group mismatch – since for the purposes of this paper the energy was divided into smaller bins, getting 500-group energy spectrum.

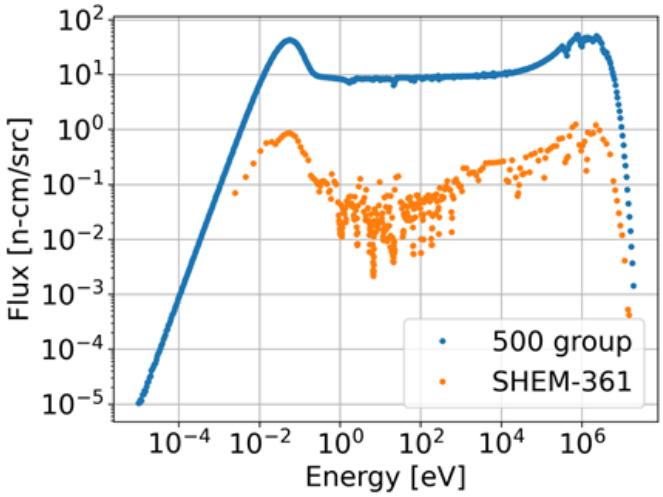

Figure 3 – Neutron spectrum of a Design-Basis Core (blue),
compared with SHEM-361 energy group (orange)

Neutron flux and heat distribution, normalized on a 900 kW reactor output, are presented in Figure 4. The temperature distribution in Figure 4 (b) is concentrated on the fuel pins, with the coldest ones in the center of the assembly, confirming that heat is generated only in the fuel zones. The relatively colder pins are located in the center of the core and the heat increase is shown to have a radially outward direction, where at the edges the hottest pins can be seen. This trend can be observed in [35, 36], while other studies show exactly the inverse behavior [12, 16].

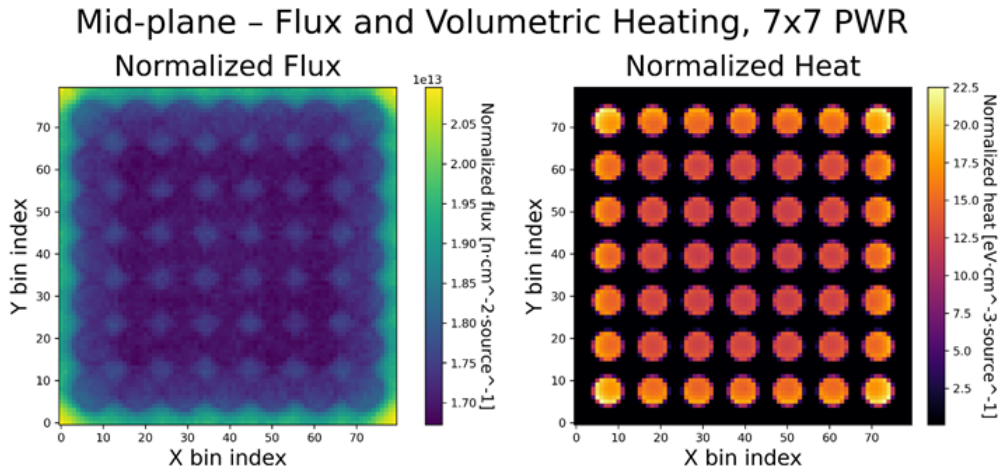

Figure 4 – Normalized flux (a) and heat (b) distribution of the core assembly.
Scale is as follows: colder colors – lower flux/temperature

3.2. Thermal-hydraulics, solid mechanics and fuel safety

3.2.1. Temperature

Figures 5 (a) and (b) present the temperature contours in the yx plane at 0.2 s and 0.8 s, respectively, following the application of the maximum volumetric heat source in the fuel. At 0.2 s, the highest temperatures are confined to the fuel region, while a clear radial temperature gradient develops across

the fuel–cladding interface and into the surrounding coolant. As time increases to 0.8 s, the heated zone expands radially, and the temperature increases throughout the fuel and cladding and reaching a maximum, indicating enhanced heat diffusion and thermal penetration into the adjacent materials. Figure 4 (c) shows the temperature profiles along the fuel rod for different time periods (0–0.8 s). The profiles reveal a relatively uniform temperature within the fuel at early times, followed by a gradual decrease across the cladding and a sharp temperature drop within the coolant region. The normalized neutron flux and volumetric heat distributions for the 7×7 PWR assembly are presented in Figure 4. The thermal field is primarily concentrated within the fuel regions, confirming that volumetric heat generation occurs exclusively inside the fuel pins. The radial heat distribution reveals comparatively lower temperatures in the central region of the assembly and progressively increasing temperatures toward the peripheral fuel pins, where the maximum thermal intensity is observed. This behavior is associated with the spatial neutron-flux distribution and geometric characteristics of the assembly. Similar thermal trends have been reported in previous studies of thorium-based and conventional fuel systems, although several investigations have demonstrated inverse radial distributions depending on fuel composition and reactor configuration [35].

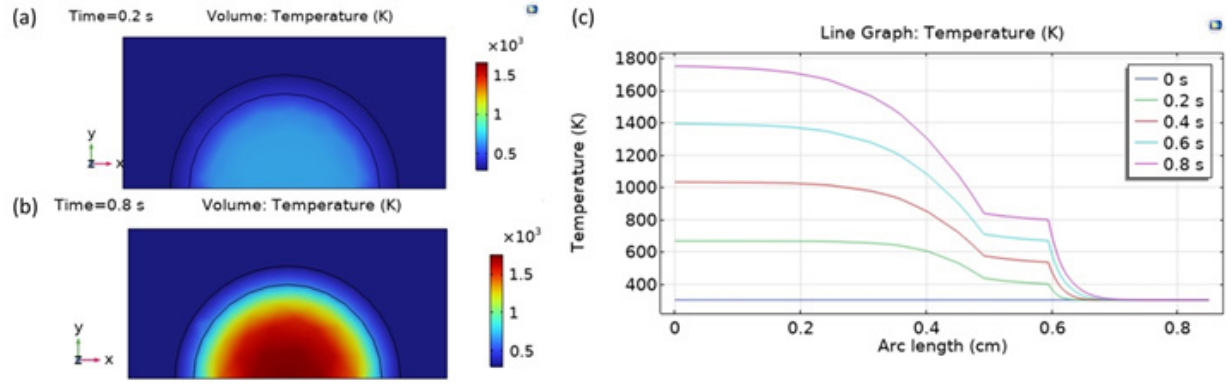

Figure 5 – The temperature profile along the y-x direction at (a) 0.2s and (b) 0.8s;
(c) the temperature distribution through different materials of the fuel rod after application of the maximum heat source for different times (from 0 to 0.8 seconds)

3.2.2. Coolant velocity

Figure 6 (a) presents a three-dimensional slice of the velocity magnitude at t=0.8 s. The color map indicates a predominantly uniform flow along the axial direction, with higher velocities concentrated toward the central region of the channel and lower velocities near the walls. This distribution reflects the combined effects of channel geometry and viscous boundary layers, resulting in a developed velocity profile along the flow direction. Figure 6 (b) shows the corresponding velocity magnitude along the rod length at two different times, 0.2 s and 0.8 s. At 0.2 s, the velocity profile remains relatively flat, indicating that the flow is still developing. As time increases to 0.8 s, the velocity increases along the channel length, with a noticeable rise near the outlet region up to 1.1 m/s. The higher velocities observed at later times suggest flow acceleration due to thermal effects and coupling with heat transfer, while the sharp increase near the end of the channel highlights the outlet and boundary influences. However, no variation in pressure is observed over the 0.8 s interval, despite the increase in heat sources. Heat removal from the cladding occurs through the surrounding coolant domain. In the coolant, the heat transfer is governed by the coupled heat-transfer and fluid-flow physics. Therefore, the coolant removes the heat mainly by forced convection along the axial direction. The calculated velocity field reflects the imposed inlet/outlet flow conditions and the development of the coolant flow inside the channel. Thus, the temperature distribution results from the combined effect of internal fuel heat generation, conductive heat transfer through the solid fuel and cladding, and convective heat removal by the coolant. A nearly unchanged pressure indicates that, under the present modeling assumptions, the coolant flow remains stable during the short heating transient.

However, a more realistic assessment of pressure evolution would require a full-assembly or system-level thermal-hydraulic model with realistic inlet/outlet pressure losses, pump characteristics, and feedback between coolant heating, density variation, and flow resistance.

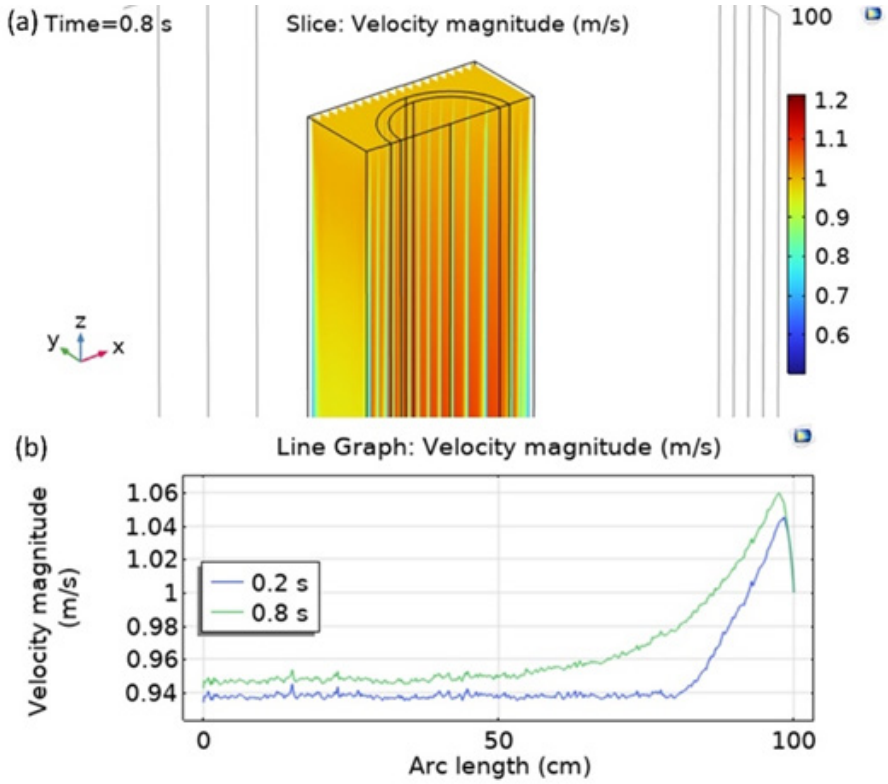

Figure 6 – (a) 3D slice of the velocity magnitude at t=0.8 s;
(b) corresponding velocity magnitude along the rod at t=0.2 s and t=0.8 s.

3.2.3. Mechanical stresses

Figures 7 (a) and (b) show the spatial distribution of von Mises stress at 0.2 s and 0.8 s, respectively. As time increases to 0.8 s, the magnitude of von Mises stress increases significantly throughout the active zone, reflecting the development of thermally induced stresses due to temperature gradients and constrained thermal expansion. Higher stress concentrations are observed along the axial direction and near geometrical or material transition regions, where mechanical constraints and thermal gradients are more pronounced. Figure 7 (c) shows the corresponding von Mises stress profiles along the rod length for both time instants. The stress remains nearly constant along most of the active zone, indicating a relatively uniform mechanical loading, while a noticeable increase in stress magnitude is observed at later times. The higher stress levels confirm the cumulative effect of thermal loading over time.

Figures 8 (a) and (b) present the spatial distribution of volumetric strain at 0.2 s and 0.8 s, respectively. At 0.2 s, the strain field is already dominated by positive volumetric strain, indicating thermal expansion of the material as heat is deposited in the active zone. The highest strain values are concentrated in the central region, while lower strain magnitudes appear near the outer region, reflecting the presence of mechanical constraints and cooler surrounding regions. At 0.8 s the magnitude of volumetric strain increases noticeably throughout the active zone, demonstrating the cumulative effect of continued heating. The expansion becomes more pronounced and spatially extended, while the overall strain pattern remains similar, suggesting a stable deformation mode governed by the temperature distribution rather than abrupt mechanical instabilities. Figure 8 (c) shows the volumetric strain profiles along the rod length for both time instants. The strain remains relatively uniform along most of the active zone, with higher values observed at 0.8 s compared

to 0.2 s. Minor fluctuations along the arc length may be attributed to geometric features, material interfaces, or numerical discretization effects. A small reduction near the boundaries indicates the influence of mechanical constraints imposed at the top and bottom surfaces. An increased volumetric strain in the fuel compared to the cladding material was also observed in the literature [36].

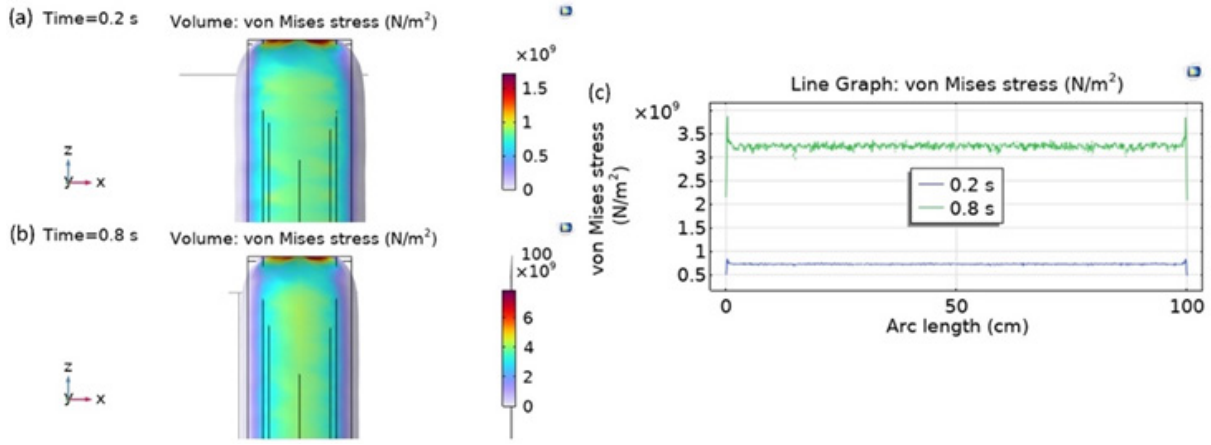

Figure 7 – Spatial distribution of von Mises stress at (a) 0.2 s and (b) 0.8 s, respectively; (c) the corresponding von Mises stress profiles along the rod length for both time instants

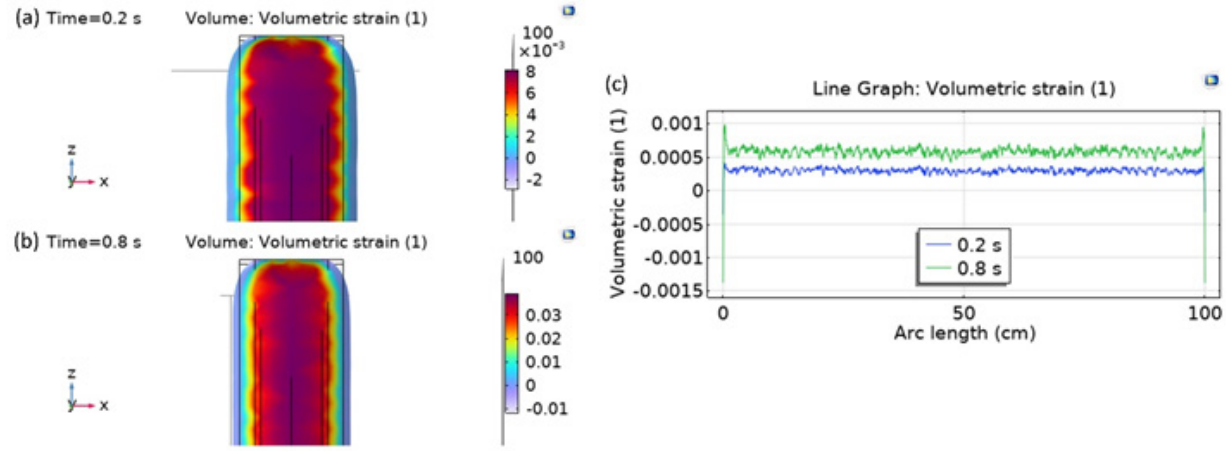

Figure 8 – Spatial distribution of volumetric strain at (a) 0.2 s and (b) 0.8 s, respectively; (c) volumetric strain profiles along the rod length for both time instants

Figures 9 (a) and (b) show the spatial distribution of the displacement magnitude at 0.2 s and 0.8 s, respectively. At the early time of 0.2 s, the displacement is relatively small throughout the structure, indicating the initial stage of thermal expansion following heat deposition with. The deformation is distributed smoothly along the axial direction, with minimal distortion near the boundaries due to mechanical constraints. At 0.8 s, the displacement magnitude increases significantly, reflecting the cumulative effect of sustained heating. The deformation becomes more pronounced in the central region of the active zone, while lower displacement values are observed near the top and bottom boundaries, consistent with the imposed structural constraints. The overall displacement pattern remains symmetric, suggesting a stable and uniform thermo-mechanical response without localized buckling or instability. Figure 9 (c) presents the displacement magnitude along the rod length for both time instants. The displacement increases gradually from the boundaries toward the mid-span, reaching a maximum near the center of the core, and then decreases toward the opposite boundary. The substantially higher displacement at 0.8 s compared to 0.2 s highlights the strong time dependence

of thermal expansion. The displacement profile suggests non-uniform deformation along the radial length, which is influenced by local thermal and mechanical loading distributions [37].

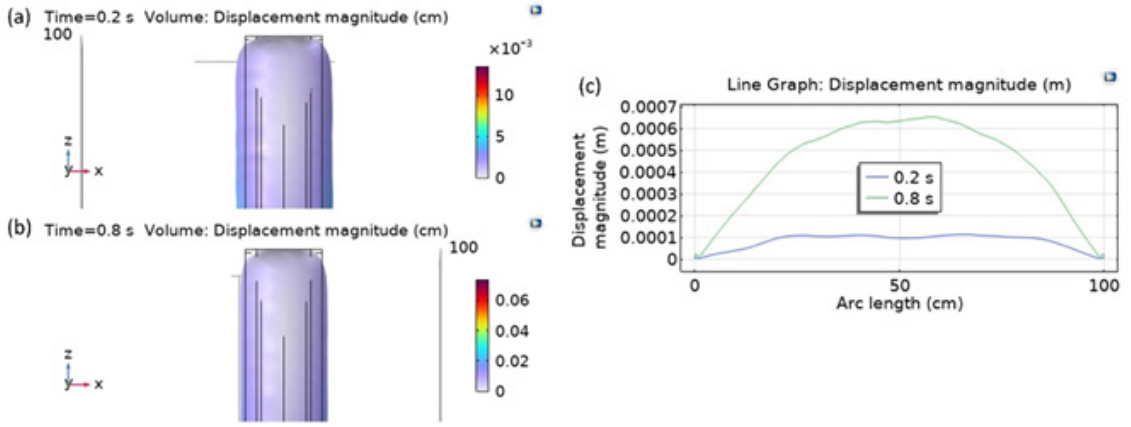

Figure 9 – Spatial distribution of the displacement magnitude at (a) 0.2 s and (b) 0.8 s, respectively; (c) displacement magnitude along the rod length for both time instants

Figures 10 (a), (b) and (c) show the von Mises stress, strain and displacement magnitude in the cladding. At 0.2 s, the stress level and displacement remain relatively low and fairly uniform along the rod length, indicating the initial response to thermal loading. As time increases to 0.8 s, the von Mises stress rises noticeably across the entire cladding, reflecting the accumulation of thermally induced stresses due to temperature gradients and constrained expansion. Slight variations near the boundaries may be attributed to geometric effects and boundary conditions, but overall, the stress distribution remains smooth, suggesting the absence of localized stress concentrations. At 0.8 s, the displacement magnitude increases significantly, reaching a maximum near the center of the rod length and decreasing toward the constrained boundaries. This symmetric displacement profile reflects thermally driven expansion constrained at the ends, leading to maximum deformation in the central region. Positive volumetric strain is observed at both time instants, indicating thermal expansion of the cladding material. The strain magnitude is consistently higher at 0.8 s than at 0.2 s, demonstrating progressive expansion as heating continues. The relatively uniform strain profile along the arc length implies that the cladding undergoes largely homogeneous volumetric deformation, with only minor fluctuations associated with numerical discretization or local thermal variations.

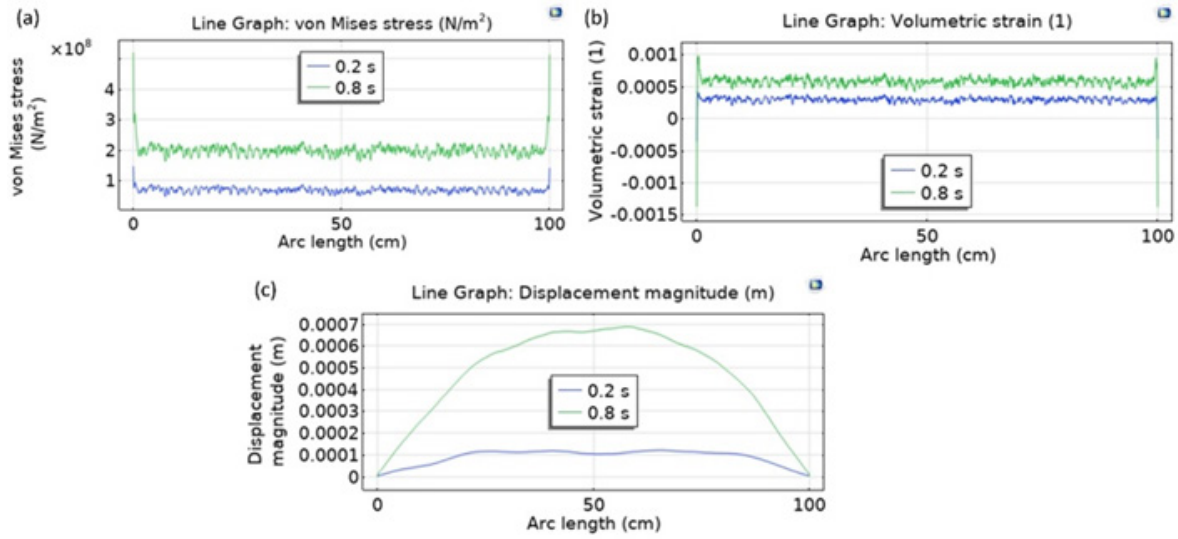

Figure 10 – (a) von Mises stress, (b) strain and (c) displacement magnitude in the cladding at 0.2 s and 0.8 s.

Unusually high values observed in temperature and stresses evaluation, while conducting a safety analysis, indicate a very high risk in designing the PWR with this material composition and power distribution. Unless comprehensive analysis has been conducted, it is early to judge the possibility of replacing uranium fuel with thorium in PWR cores. The analysis, according to the authors' opinions, should include realistic power output of the design, more detailed material composition and, possibly, feedback loop between the coupled physics processes.

4. Conclusions

A coupled neutronic, thermal-hydraulic, and thermo-mechanical analysis of a thorium-based PWR fuel assembly was successfully performed using OpenMC and COMSOL Multiphysics. The neutronic calculations provided the effective neutron multiplication factor and spatial power distribution required for transient thermal-hydraulic simulations. The obtained results demonstrated progressive temperature accumulation within the fuel region, accompanied by the development of thermal gradients, thermally induced stresses, volumetric strain, and structural displacement during transient operation.

The study confirms that coupling steady-state neutronics with transient thermal-hydraulic analysis represents a computationally efficient approach for multiphysics reactor simulations while preserving the dominant physical interactions governing reactor behavior. At the same time, the elevated temperature and stress values obtained during short transient periods indicate the necessity for further refinement of the current model, including more realistic power distributions, improved thermal-hydraulic boundary conditions, and incorporation of additional physics feedback mechanisms.

Future work will focus on extending the model to full-core reactor configurations and implementing more advanced coupled multiphysics approaches to improve the realism and predictive capability of thorium-based PWR safety analyses.

Acknowledgment. The article includes the results of research carried out within the framework of project-targeted funding under the project IRN BR24993225 funded by the Committee of Science of the Ministry of Science and Higher Education of the Republic of Kazakhstan.

REFERENCES

1 World Nuclear Association. Thorium. URL: https://world-nuclear.org/information-library/current-and-future-generation/thorium

2 Oak Ridge National Laboratory. Molten-Salt Reactor Experiment 1965–1972 (Oak Ridge, TN: ORNL, 2015). URL: https://web.archive.org/web/20160303211133if_/https://dl.dropboxusercontent.com/u/15726934/Historic_Molten_Salt_Reactor_Experiment_Brochure_ORNL_1965-1972.pdf

3 Carter, L.L. Monte Carlo Code Development in Los Alamos. Los Alamos Scientific Laboratory Report (March 1975).

4 James, M.R. MCNPX 2.7.x – New Features Being Developed. Los Alamos National Laboratory Technical Report.

5 Romano, P.K., Horelik, N.E., Herman, B.R., Nelson, A.G., Forget, B., and Smith, K. OpenMC: A State-of-the-Art Monte Carlo Code for Research and Development. Annals of Nuclear Energy, 82, 90–97 (2015). https://doi.org/10.1016/j.anucene.2014.07.048

6 Brown, D.A., Chadwick, M.B., Capote, R., Kahler, A.C., Trkov, A., Herman, M.W., Sonzogni, A.A., Danon, Y., Carlson, A.D., Dunn, M., et al. ENDF/B-VIII.0: The 8th Major Release of the Nuclear Reaction Data Library with CIELO-Project Cross Sections, New Standards and Thermal Scattering Data. Nuclear Data Sheets, 148, 1–142 (2018). https://doi.org/10.1016/j.nds.2018.02.001

7 Plompen, A.J.M., Cabellos, O., De Saint Jean, C., Fleming, M., Algora, A., Angelone, M., Archier, P., et al. The Joint Evaluated Fission and Fusion Nuclear Data Library, JEFF-3.3. European Physical Journal A, 56 (7), 181 (2020). https://doi.org/10.1140/epja/s10050-020-00141-9

8 Tsige-Tamirat, H. Neutronics Assessment of the Use of Thorium Fuels in Current Pressurized Water Reactors. Progress in Nuclear Energy, 53 (6), 717–721 (2011). https://doi.org/10.1016/j.pnucene.2010.12.001

9 Trellue, H.R., Bathke, C.G., and Sadasivan, P. Neutronics and Material Attractiveness for PWR Thorium Systems Using Monte Carlo Techniques. Progress in Nuclear Energy, 53 (6), 698–707 (2011). https://doi.org/10.1016/j.pnucene.2011.02.002

10 Chaudri, K.S., Tian, W., Su, G., and Qiu, S. Coupled Neutronics/Thermal Hydraulics Evaluation for Thorium Based Fuels in Thermal Spectrum SCWR. Progress in Nuclear Energy, 68, 55–64 (2013). https://doi.org/10.1016/j.pnucene.2013.04.005

11 Arzhannikov, A.V., Shmakov, V.M., Modestov, D.G., Bedenko, S.V., Prikhodko, V.V., Lutsik, I.O., and Shamanin, I.V. Facility to Study Neutronic Properties of a Hybrid Thorium Reactor with a Source of Thermonuclear Neutrons Based on a Magnetic Trap. Nuclear Engineering and Technology, 52 (11), 2460–2470 (2020). https://doi.org/10.1016/j.net.2020.04.017

12 Kumar, E.R.S.A., Pancholi, M.K., Darnowski, P., and Dzido, A. Neutronic Performance of a Thorium Based Mixed Oxide Fuel in a Burner Sodium-Cooled Fast Reactor. Energy, 212, 118744 (2020). https://doi.org/10.1016/j.energy.2020.118744

13 Galahom, A.A., Mohsen, M.Y., and Amrani, N. Explore the Possible Advantages of Using Thorium-Based Fuel in a Pressurized Water Reactor (PWR). Part 1: Neutronic Analysis. Nuclear Engineering and Technology, 54 (1), 1–10 (2022). https://doi.org/10.1016/j.net.2021.07.012

14 Li, J., Li, X., and Cai, J. Neutronic Characteristics and Feasibility Analysis of Micro-Heterogeneous Duplex ThO_2-UO_2 Fuel Pin in PWR. Nuclear Engineering and Design, 382, 111382 (2021). https://doi.org/10.1016/j.nucengdes.2021.111382

15 Kabach, O., Chetaine, A., Benchrif, A., Amsil, H., and El Banni, F. A Comparative Analysis of the Neutronic Performance of Thorium Mixed with Uranium or Plutonium in a High-Temperature Pebble-Bed Reactor. International Journal of Energy Research, 45 (11), 16824–16841 (2021). https://doi.org/10.1002/er.6863

16 Mirvakili, S.M., Kavafshary, M.A., and Vaziri, A.J. Comparison of Neutronic Behavior of UO_2, (Th-233U)O_2 and (Th-235U)O_2 Fuels in a Typical Heavy Water Reactor. Nuclear Engineering and Technology, 47 (3), 315–322 (2015). https://doi.org/10.1016/j.net.2014.12.005

17 Tucker, L.P., Alajo, A., and Usman, S. Thorium-Based Mixed Oxide Fuel in a Pressurized Water Reactor: A Beginning-of-Life Feasibility Analysis with MCNP. Annals of Nuclear Energy, 76, 323–334 (2015). https://doi.org/10.1016/j.anucene.2014.10.020

18 Pillai, C.G.S., and Raj, P. Thermal Conductivity of ThO_2 and Th0.98U0.02O_2. Journal of Nuclear Materials, 277 (1), 116–119 (2000). https://doi.org/10.1016/S0022-3115(99)00237-8

19 Kutty, T.R.G., Kulkarni, R.V., Sengupta, P., Khan, K.B., Bhanumurthy, K., Sengupta, A.K., Panakkal, J.P., Kumar, A., and Kamath, H.S. Development of CAP Process for Fabrication of ThO_2–UO_2 Fuels. Part II: Characterization and Property Evaluation. Journal of Nuclear Materials, 373 (1–3), 309–318 (2008). https://doi.org/10.1016/j.jnucmat.2007.06.011

20 Bakker, K., Cordfunke, E.H.P., Konings, R.J.M., and Schram, R.P.C. Critical Evaluation of the Thermal Properties of ThO_2 and Th1−yUyO_2 and a Survey of the Literature Data on Th1−y$PuyO_2$. Journal of Nuclear Materials, 250 (1), 1–12 (1997). https://doi.org/10.1016/S0022-3115(97)00241-9

21 Tyagi, A.K., Mathews, M.D., Ambekar, B.R., and Ramachandran, R. Thermal Expansion of ThO_2–2, 4 and 6 wt.% UO_2 by HT-XRD. Thermochimica Acta, 421 (1–2), 69–71 (2004). https://doi.org/10.1016/j.tca.2004.04.025

22 Tyagi, A.K., and Mathews, M.D. Thermal Expansion of ThO_2–2 wt.% UO_2 by HT-XRD. Journal of Nuclear Materials, 278 (1), 123–125 (2000). https://doi.org/10.1016/S0022-3115(99)00277-9

23 Anthonysamy, S., Panneerselvam, G., Bera, S., Narasimhan, S.V., and Vasudeva Rao, P.R. Studies on Thermal Expansion and XPS of Urania–Thoria Solid Solutions. Journal of Nuclear Materials, 281 (2–3), 308–316 (2000). https://doi.org/10.1016/S0022-3115(00)00185-9

24 Ghosh, P.S., Somayajulu, P.S., Krishnan, K., Pathak, N., Arya, A., and Dey, G.K. Thermal Expansion and Thermal Conductivity of (Th,U)O_2 Mixed Oxides: A Molecular Dynamics and Experimental Study. Journal of Alloys and Compounds, 650, 165–177 (2015). https://doi.org/10.1016/j.jallcom.2015.07.260

25 Xiao, H., Long, C., Tian, X., Chen, H., and Duan, X. Effect of Thorium Addition on the Thermophysical Properties of Uranium Dioxide: Atomistic Simulations. Materials & Design, 96, 335–340 (2016). https://doi.org/10.1016/j.matdes.2016.02.019

26 Griggs, D.P., Henry, A.F., and Kazimi, M.S. Development of a Three-Dimensional Two-Fluid Code with Transient Neutronic Feedback for LWR Applications. Massachusetts Institute of Technology Technical Report (1981).

27 Mahadevan, V.S. High Resolution Numerical Methods for Coupled Non-Linear Multi-Physics Simulations with Applications in Reactor Analysis. PhD Dissertation, Texas A&M University, College Station, TX, USA (2010).

28 Pijls, T. Developing a GPU-Accelerated Filter-Matrix Lattice Boltzmann Multiphysics Tool for the Transient Thermal-Hydraulics and Neutronics of a Molten Salt Fast Reactor Core. MSc Thesis, Delft University of Technology, Delft, The Netherlands (2025). URL: https://martinrohde.nl/theses/msc/MSc_Thomas_Pijls.pdf

29 Hanumantharao, G., Vijay, S., and Venkateswara Rao, M. Transient Heat Transfer Analysis for Optimum Temperature Distribution to Reduce Thermal Stresses. International Journal of Engineering Research and Technology, 1, 1–7 (2012).

30 Fuertes-Miquel, V.S. Transient Flows: Mathematical Models, Laboratory Tests, Protection Elements and Systems. Water, 17, 1454 (2025). https://doi.org/10.3390/w17111454

31 Hu, R., Fang, J., Nunez, D., Tano, M., Giudicelli, G., and Salko, R. Development of Integrated Thermal Fluids Modeling Capability for MSRs. Argonne National Laboratory Report ANL/NSE-22/56 (2022).

32 Mohsen, M.Y.M., Abdel-Rahman, M.A.E., and Galahom, A.A. Ensuring the Possibility of Using Thorium as a Fuel in a Pressurized Water Reactor (PWR). Nuclear Science and Techniques, 32, 137 (2021). https://doi.org/10.1007/s41365-021-00981-0

33 Hammer, R.R. Zircaloy-4, Uranium Dioxide, and Materials Formed by Their Interaction: A Literature Review with Extrapolation of Physical Properties to High Temperatures. Idaho Nuclear Corporation Report IN-1093 (Idaho Falls, ID, USA, 1967).

34 Shields, A.E., Hernandez, S.E.R., and de Leeuw, N.H. Theoretical Analysis of Uranium-Doped Thorium Dioxide: Introduction of a Thoria Force Field with Explicit Polarization. AIP Advances, 5, 087118 (2015). https://doi.org/10.1063/1.4928438

35 Jiao, G., Xia, G., Zhu, H., Zhou, T., and Peng, M. Thermal-Mechanical Coupling Characteristics and Heat Pipe Failure Analysis of Heat Pipe Cooled Space Reactor. Annals of Nuclear Energy, 192, 110025 (2023). https://doi.org/10.1016/j.anucene.2023.110025

36 Mohsen, M.Y.M., Soliman, A.Y., and Abdel-Rahman, M.A.E. Thermal-Hydraulic and Solid Mechanics Safety Analysis for VVER-1000 Reactor Using Analytical and CFD Approaches. Progress in Nuclear Energy, 130, 103568 (2020). https://doi.org/10.1016/j.pnucene.2020.103568

37 Mohsen, M.Y.M., Abdel-Rahman, M.A.E., Hassan, M.S., and Galahom, A.A.G. Searching for the Most Optimum Burnable Absorbers (BAs) for AP-1000 from the Neutronic, Thermal-Hydraulic, and Solid Mechanics Points of View. Nuclear Engineering and Design, 391, 111728 (2022). https://doi.org/10.1016/j.nucengdes.2022.111728

[1]Арынгазин А.,
магистр, ORCID ID: 0009-0007-7861-4917,
e-mail: ansar.aryngazin@nu.edu.kz
[1]Курбанова Б.,
магистр, ORCID ID: 0000-0003-0928-521X,
e-mail: bayan.kurbanova@nu.edu.kz
[2]Сизюк Ю.,
PhD, e-mail: yuriy.sizyuk@nu.edu.kz
[3]Темирбаева А.,
магистр, ORCID ID: 0000-0002-9526-3617,
e-mail: assem.zkgmu@gmail.com
[1]Алсар Ж.,
PhD, ORCID ID: 0000-0001-7287-7555,
e-mail: zhanna.alsar@nu.edu.kz
[1]*Инсепов З.,
PhD, жетекші зерттеуші, адъюнкт-профессор, ORCID ID: 0000-0002-8079-6293,
*e-mail: zinsepov@nu.edu.kz

[1]Назарбаев университетінің зерттеу басқармасы, Астана қ., Қазақстан;
[2]Механикалық ядролық инженерия кафедрасы, вирджиния достастық университеті, Вирджиния, АҚШ;
[3]Гумилев атындағы Еуразия ұлттық университеті, Астана қ., Қазақстан;
[4]Ядролық инженерия мектебі, Пердью университеті, Индиана, АҚШ.

ТОРИЙ ОТЫНЫ ҚОЛДАНЫЛАТЫН ҚЫСЫМДАҒЫ СУ РЕАКТОРЫНЫҢ НЕЙТРОНДЫҚ-ФИЗИКАЛЫҚ ЖӘНЕ ЖЫЛУ-ГИДРАВЛИКАЛЫҚ СИПАТТАМАЛАРЫН ЗЕРТТЕУ

Аңдатпа

Жұмыста жылу-гидравликалық үдерістердің және қатты дене механикасы құбылыстарының динамикасы COMSOL Multiphysics бағдарламалық кешенінде соңғы элементтер әдісі негізінде модельденді. Нейтрондық-физикалық сипаттамаларды зерттеу үшін OpenMC бағдарламалық пакеті стационарлық нейтроника жуықтауында қолданылды. Торий негізіндегі реактордың белсенді аймағын оңтайландыру мақсатында салқындатқыш ретінде жоғары қысымды жеңіл су пайдаланылды. Белсенді аймақта торий қосылыстарымен толтырылған 49 отын штангасы орналастырылды. OpenMC пакетінде жүзеге асырылған Монте-Карло әдісі арқылы нейтрондардың тасымалдануын модельдеу нәтижесінде қарастырылған реактор үлгісінің тиімді көбейту коэффициенті ($k_e$ff) мен қуаттың таралуы анықталды. Жылу-гидравликалық есептеулер нәтижесінде температуралық профильдер мен ағын жылдамдығының мәндері алынды, ал қатты дене механикасы бойынша жүргізілген талдау нәтижесінде кернеулер мен деформациялардың кеңістіктік таралуы анықталды. Алынған нәтижелер стационарлық нейтроника мен өтпелі жылу-гидравликаны байланыстыра есептеу әдісін қолданудың тиімділігін растады.

Түйін сөздер: ядролық реактор физикасы, торий отыны, нейтроника, термиялық гидравлика, қатты дене механикасы, COMSOL, OpenMC.

[1]Арынгазин А.,
MSc, ORCID ID: 0009-0007-7861-4917,
e-mail: ansar.aryngazin@nu.edu.kz,
[1]Курбанова Б.
PhD, ORCID ID: 0000-0003-0928-521X,
e-mail: bayan.kurbanova@nu.edu.kz,
[2]Сизюк Ю.,
PhD, e-mail: yuriy.sizyuk@nu.edu.kz,
[3]Темирбаева А.,
M.Sc. ORCID ID: 0000-0002-9526-3617,
e-mail: assem.zkgmu@gmail.com
[1]Алсар Ж.,
PhD, ORCID ID: 0000-0001-7287-7555,
e-mail: zhanna.alsar@nu.edu.kz
[1*]Инсепов З.,
доктор наук, PhD, адъюнкт-профессор, ORCID ID: 0000-0002-8079-6293,
*e-mail: zinsepov@nu.edu.kz

[1]Исследовательская администрация Назарбаевского университета, г. Астана, Казахстан
[2]Кафедра машиностроения и ядерной инженерии, Университет Содружества Вирджинии, Вирджиния, США
[3]Евразийский национальный университет им. Л.Н. Гумилева, г. Астана, Казахстан
[4]Школа ядерной инженерии, Университет Пердью, Индиана, США

ИССЛЕДОВАНИЕ НЕЙТРОНИКИ И ТЕПЛОГИДРАВЛИКИ РЕАКТОРА С ВОДОЙ ПОД ДАВЛЕНИЕМ И ТОПЛИВОМ НА ОСНОВЕ ТОРИЯ

Аннотация

В данной работе динамика тепло-гидравлических явлений, а также явлений механики твердого тела была смоделирована методом конечных элементов с использованием Comsol Multiphysics. Для изучения нейтроники был применен OpenMC в приближении стационарной нейтроники. Для оптимизации активной зоны ториевого реактора в качестве охладителя использовалась легкая вода под высоким давлением. В активной зоне располагались 49 топливных стержней, заполненные соединениями тория, организованные в виде регулярной – решеточной геометрии. Моделирование переноса нейтронов методом Монте-Карло в пакете OpenMC позволило получить эффективное значение коэффициента размножения k_eff и пространственное распределение мощности рассматриваемой модели. Были получены детальные тепло- и гидравлические расчеты – температурный и скоростные профили, в то время как механика твердого тела определила пространственное распределение напряжений и деформаций. Результаты подтвердили применимость и эффективность использования метода совмещения стационарной нейтроники с термогидравликой и структурного анализа для оценки и оптимизации ториевых реакторов с водным охлаждением.

Ключевые слова: физика ядерных реакторов, ториевое топливо, нейтронная физика, теплогидравлика, механика твердого тела, COMSOL, OpenMC.